# Surface-Modified Hydrogels for Chemoselective Bioconjugation

**Kyle N. Plunkett, Aveek N. Chatterjee, N. R. Aluru,* and Jeffrey S. Moore***

*The Beckman Institute for Advanced Science and Technology, The University of Illinois at Urbana−Champaign, Urbana, Illinois 61801*

*Received August 8, 2003; Revised Manuscript Received September 10, 2003*

ABSTRACT: Patterned hydrogels of glycerol monomethacrylate (GMM)-*co*-acrylic acid (AA) were prepared in microchannels using an in situ photopolymerization method. Oxidation of the hydrogel was accomplished using aqueous sodium periodate ($NaIO_4$) to produce an aldehyde functionalized surface. The depth of oxidation, characterized by confocal microscopy after conjugation with a fluorescent dye, was controlled by varying the $NaIO_4$ concentration, reaction time, and temperature. Hydrogel oxidation was modeled by combining the Nernst−Planck, Poisson, Arrhenius, and rate equations. The modeling studies suggest that the glycol oxidation reaction and the diffusion of oxidant into the hydrogel are competitive factors in determining the oxidation depth. Once modified, these hydrogels have the ability to covalently bind small molecules and biomolecules to their surface under mild, aqueous conditions. For example, fluorescently labeled bovine serum albumin (FITC-BSA) was site-specifically conjugated to the surface of a photopatterned hydrogel via reductive amination.

## Introduction

Surface modifications of polymeric materials have found importance in a multitude of applications as they provide the opportunity to transform inexpensive polymers with desirable bulk properties into specialized materials.[1] Surface modifications have been employed to alter the polymer's chemical composition, hydrophilicity, cross-link density, biocompatibility, and adhesion.[1] Relevant to the work described herein, polymer modification techniques that utilize solution-phase, organic reactions to perform oxidations,[2] reductions,[3] and couplings[4] at the polymer surface have previously been reported. Through these conventional transformations, the polymer can be tailored to display the chemical and physical characteristics needed for a specific application.

Hydrogels are materials that can benefit from surface modifications as they are typically prepared from simple monomers and exhibit high water affinity. Typical monomers used for hydrogel preparation comprise of alcohol, amine, or carboxylic acid pendant groups that can be modified through common solution-phase transformations to expand the functionality of the polymer network. These modified hydrogels have been utilized for increasing biocompatibility[5] and for controlled hydrogel swelling with potential applications ranging from controlled drug delivery[6] to biosensing.[7]

To increase hydrogel biocompatibility, hydrolysis of poly(hydroxyethyl) methacrylate hydrogels with aqueous solutions of NaOH at >90 °C led to surface localized carboxylic acid groups.[5] Other work has focused on the immobilization of lipids to microscopic hydrogel surfaces to create "artificial cells"[8] and to create mimics of the secretory granule for drug delivery.[6,9] More recently, pH-responsive hydrogels with covalent attached alkyl chains where similarly shown to maintain a ion concentration gradient between the interior and exterior of the hydrogel that could be disrupted through physical or chemical means.[10,11] While these examples show that hydrogels can be surface modified, there is need for a detailed understanding of the modification process. Additionally, the development of new hydrogels that can be modified in a controlled manner with minimal perturbation of the hydrogel properties while setting in place the chemistry that would enable aqueous conjugations to proteins, nucleic acids, or other bioactive molecules would be beneficial for many applications.[7]

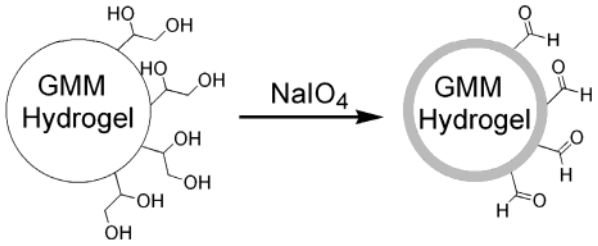


**Figure 1.** Schematic representation of the $NaIO_4$ oxidation of a cylindrical GMM hydrogel. Oxidation, which is located near the surface, preserves the bulk properties of the hydrogel while providing a reactive shell for the chemoselective ligation of molecules.

Herein, we describe a hydrogel that is ideally suited for surface localized chemoselective ligation. Chemoselective ligation refers to controlled coupling of two mutually and uniquely reactive functional groups in aqueous solutions and is typically used for the conjugation of peptides or other biological molecules.[12] Hydrogels designed for chemoselective ligation will have utility for biochip fabrication since biomolecules can be immobilized in their native states. This hydrogel is based on the 1,2-diol containing monomer glycerol monomethacrylate (GMM).[13] Hydrogels from GMM are easily prepared inside a microchannel following in situ photopolymerization procedures that we have previously described for other hydrogel systems.[11] GMM hydrogels have previously been shown to behave as ideal elastic networks with high water affinity and therefore provide an excellent scaffold for aqueous reactions and immobilization.[13] Oxidation of the hydrogel surface with sodium periodate ($NaIO_4$) produces an aldehyde-rich exterior with a diol-functionalized interior (Figure 1).

* To whom correspondence should be addressed: e-mail aluru@uiuc.edu or moore@scs.uiuc.edu; phone (217) 244-4024; Fax (217) 244-8068.

10.1021/ma035166+ CCC: $25.00 
Published on Web 10/25/2003

**Scheme 1. Chemoselective Ligation of an Aldehyde with an Aminooxy Functionized Molecule**[a]

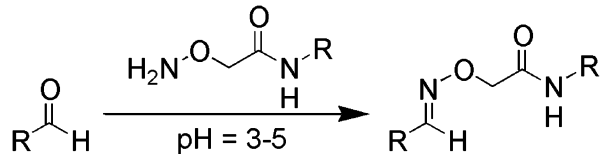


[a] Reactions are accomplished in aqueous buffers at room temperature.

**Scheme 2. Oxidation of a 1,2-Diol with $NaIO_4$**

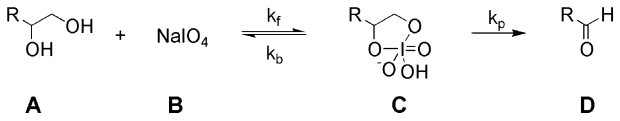


This strategy maintains the desired bulk properties of the GMM hydrogel, while placing chemically reactive functionality at the surface. Once the aldehyde functionality is installed, the reactive surface allows for the chemoselective ligation of a variety of molecules including aminooxy, hydrazide, or N-terminated cysteine-functionalized molecules (Scheme 1)[12,14] as well as the conjugation of amines through typical reductive amination techniques.[15]

Described below is a systematic study of the surface oxidation reaction on GMM hydrogels. One of the aims was to create a thin, concentrated layer of aldehyde functionality on the hydrogel perimeter without disturbing the interior properties. Reaction conditions such as temperature, oxidant concentration, flow rate, and reaction time of oxidation were varied to find the dependence on the oxidation depth. Computational modeling has been employed to provide insight into the competition between the rate of diffusion of $NaIO_4$ into the hydrogel and the rate of conversion of diol to aldehyde. Using optimized procedures, a fluorescently labeled protein was immobilized to the surface; this demonstration is an important step in creating a new pH-responsive scaffold bearing immobilized biomacromolecules.

## Mathematical Models and Simulations

**Oxidation Mechanism.** Oxidation of the 1,2-diol-containing hydrogel (GMM) was accomplished using aqueous solutions of sodium periodate ($NaIO_4$).[16,17] Because the hydrogel is a porous, water-solvated polymer network, periodate ions migrate from the exterior, oxidizing the 1,2-diols into aldehydes as they penetrate into the hydrogel. To analyze the reaction and diffusion events, a kinetic model is needed. The oxidation pathway (Scheme 2) reversibly forms an ester intermediate (C), which can either re-form starting materials (A and B) or irreversibly form the aldehyde product (D).

**Transport of Ions.** The migration of the periodate ion through the hydrogel was modeled using a coupled transient Nernst−Planck equation[18,19] and Poisson equation[20] as a one-dimensional process. The variation in concentrations of the reactants was also incorporated into the model by using the chemical rate equations for the oxidation process.[17,21−23] The total flux of ions was predicted using the Nernst−Planck equation which includes the fluxes due to the concentration gradient,

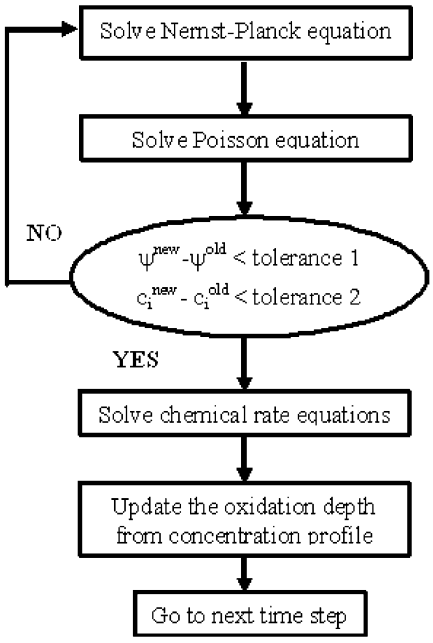


**Figure 2.** Flowchart used to solve the coupled equations within a time loop. The term "tolerance 1" and "tolerance 2" stand for the tolerance used to determine whether the solution has converged. The value was set at $10^{-5}$.

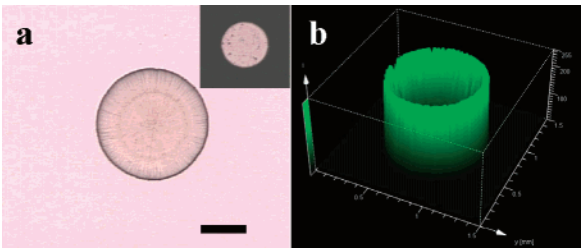


**Figure 3.** Optical micrograph of a swollen hydrogel prepared using the photomask shown as an inset (a). The resulting diameter of the hydrogel is ca. 700 $\mu$m with a height of 180 $\mu$m. Scale bar = 250 $\mu$m. A confocal microscope 3-D image (b) of a 3:1 GMM-*co*-AA hydrogel after being (i) oxidized with a 10 mM $NaIO_4$ solution for 10 min, (ii) fluorescently labeled using a 0.1 mM lucifer yellow:10 mM semicarbazide solution in pH 7.6 buffer, and (iii) deswelled by soaking the hydrogel in a pH 2.05 buffer. The green color is indicative of the fluorescence intensity emitted by lucifer yellow. Fluorescence is only observed in the areas oxidized by $NaIO_4$.

electrical migration, and convection of the oxidizing reagent:[18,19]

$$\Gamma_k = \phi\left[-\bar{D}_k\frac{\partial c_k}{\partial x} - \bar{\mu}_k z_k c_k\frac{\partial \psi}{\partial x}\right] + c_k U \qquad (1)$$

Here, $\Gamma_k$ is the flux of the $k$th ion, $\phi$ is the gel porosity, $\bar{D}_k$ is the effective diffusivity of the $k$th ion inside the hydrogel, $c_k$ is the concentration of the $k$th ionic species inside the hydrogel, $\bar{\mu}_k$ is the effective ionic mobility, $z_k$ is the valence of the $k$th ion, $\psi$ is the electric potential, $U$ is the area-averaged fluid velocity relative to the polymer network, and $x$ is the coordinate system. The Einstein relation relates diffusivity to ionic mobility[24]

$$\bar{D}_k = \frac{\bar{\mu}_k RT}{F} \qquad (2)$$

where $R$ is the universal gas constant, $T$ is the absolute temperature, and $F$ is Faraday's constant. The gel

porosity is assumed to follow the relation

$$\phi = \frac{H}{1+H} \tag{3}$$

where $H$ is the hydration state of the gel and is defined as the ratio of the volume of the fluid to the volume of the solid in the gel.[25]

Because the reaction is occurring inside a swollen hydrogel, the transport of ions is limited to regions containing fluid, and therefore an obstruction model was needed. The presence of polymer chains, which are impenetrable to mobile ions, increases the path length an ion travels, resulting in a slower diffusion rate. Mackie and Meares introduced a statistical model for the tortuosity of a cross-linked polymer membrane as seen by small ions that do not interact with the membrane.[26] According to that model, the effective diffusion rate inside the gel can be related to the diffusion in aqueous solution through an obstruction model:

$$\frac{\bar{D}_k}{D_k} = \left(\frac{H}{2+H}\right)^2 \tag{4}$$

In certain cases the effective diffusivity of ions in an ionic hydrogel may be affected by the electrostatic interaction of the ions and the fixed charges on the polymer backbone.[27] However, the effective diffusivity model given above does not take into account the effect of the electrostatic interaction between the fixed charges and the periodate ions as these interactions are negligible compared to the obstruction and tortuousity effects, which are considered in the statistical model.[28] The effective diffusivity model (eq 4) has no fitting parameter and has been used successfully by De et al.,[29] Nussbaum,[25] and Mackie et al.[26] for modeling the diffusion of ions inside an ionic hydrogel.

Applying the continuity condition in one dimension provides

$$\frac{\partial}{\partial t}(c_k) = -\frac{\partial(\Gamma_k)}{\partial x} \tag{5}$$

where $t$ is the time. From eqs 1 and 5, the continuity equation for ion concentration is given by

$$\frac{\partial}{\partial t}(c_k) = \frac{\partial}{\partial x}\left[\left(\frac{H}{1+H}\right)\left(\bar{D}_k \frac{\partial c_k}{\partial x} + \bar{\mu}_k c_k \frac{\partial \psi}{\partial x} - \frac{1+H}{H} c_k U\right)\right] \tag{6}$$

Because the convective velocity was not significant (as shown experimentally), eq 6 could be rewritten as

$$\frac{\partial}{\partial t}(c_k) = \frac{\partial}{\partial x}\left[\left(\frac{H}{1+H}\right)\left(\bar{D}_k \frac{\partial c_k}{\partial x} + \bar{\mu}_k c_k \frac{\partial \psi}{\partial x}\right)\right] \tag{7}$$

The Poisson equation was then employed to compute the electrostatic potential and the electric field:[20]

$$\frac{\partial^2 \psi}{\partial x^2} = -\frac{F}{\epsilon \epsilon_0}\left(\sum_{k=1}^{N} z_k c_k\right) \tag{8}$$

where $\epsilon_0$ is the dielectric constant of the vacuum and $\epsilon$ is the relative dielectric constant of the solvent. The coupled Nernst−Planck (eq 7) and Poisson equation (eq 8) were used to obtain the concentrations of the migrating ions. The Dirichlet boundary conditions are used for the electrical potential and the concentration of various ionic species. The bath concentration is specified as the Dirichlet boundary condition. As no external potential is applied, the specified electrical potential is zero.

**Reactions.** From Scheme 2 the net rate of formation of intermediate C (i.e., the ester) is given by

$$\frac{\partial[\mathrm{C}]}{\partial t} = k_\mathrm{f}[\mathrm{A}][\mathrm{B}] - k_\mathrm{b}[\mathrm{C}] - k_\mathrm{p}[\mathrm{C}] \tag{9}$$

and the net rate of formation of product D (i.e., the aldehyde) is given by

$$\frac{\partial[\mathrm{D}]}{\partial t} = k_\mathrm{p}[\mathrm{C}] \tag{10}$$

Finally, knowing that the concentrations of all species (i.e., starting materials, intermediates, and products) must be equal to the initial concentration, we get the following equation:

$$[\mathrm{A}] + [\mathrm{C}] + [\mathrm{D}] = [\mathrm{A}]_0 \tag{11}$$

where $[\mathrm{A}]_0$ is the initial concentration of the diol (A) and was kept constant (1.75 M) for all cases.[30]

Combination of eqs 9−11 provided the following second-order partial differential equation with respect to [D]:

$$\frac{\partial^2[\mathrm{D}]}{\partial t^2} + \frac{\partial[\mathrm{D}]}{\partial t}\{k_\mathrm{b} + k_\mathrm{p} + k_\mathrm{f}[\mathrm{B}]\} + [\mathrm{D}]\{k_\mathrm{f}[\mathrm{B}]k_\mathrm{p}\} = k_\mathrm{f}[\mathrm{A}]_0[\mathrm{B}]k_\mathrm{p} \tag{12}$$

After using eq 7 to obtain the concentration of diffused periodate, eq 12 was used to obtain the concentration profile of the aldehyde, which is the final oxidized product. The two initial conditions for the kinetic equations (eq 12) are $[\mathrm{D}] = 0$ and $\mathrm{d}[\mathrm{D}]/\mathrm{d}t = 0$. The second condition is valid because $\mathrm{d}[\mathrm{D}]/\mathrm{d}t \propto [\mathrm{C}]$ and [C] is zero at $t = 0$. To obtain the time derivative of periodate ion (i.e., [B]), backward differencing in time was used.

We assume that the reaction rates are related to the temperature by the Arrhenius equation where three separate activation energy parameters are needed for the three rate constants ($k_\mathrm{f}$, $k_\mathrm{b}$, and $k_\mathrm{p}$) as shown in Scheme 2. Previously reported experimental values of the activation energy parameters were used.[17] The dependence of the reaction rate constants and the activation energy parameter on the concentration of the diol or periodate species was neglected as the concentration of diol was significantly higher than that of the periodate ions.[22]

As the governing equations of the model just described are coupled to each other, analytical solution of these equations is impossible. Rather, the finite cloud method was used for solving the governing equations numerically.[31,32] Figure 4 shows the iterative process used to solve the coupled equations. First, the Nernst−Planck equation (eq 7) is solved to find the concentration of periodate ions inside the hydrogel. With the concentrations of the various ions in hand, the Poisson equation (eq 8) is solved to compute the electrical potential and the electrical field. Since these two equations (i.e., the Nernst−Planck equation and the Poisson equation) are coupled, they are solved iteratively to obtain a self-

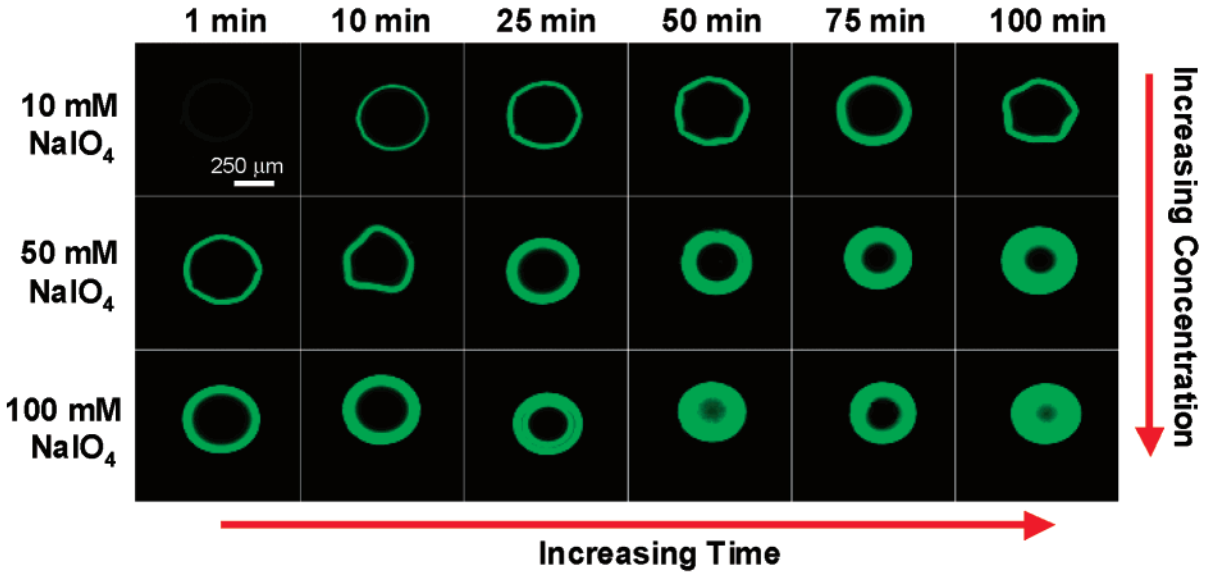


**Figure 4.** Confocal images of 18 lucifer yellow-labeled hydrogels oxidized for different times at various $NaIO_4$ concentrations. The oxidation depth visibly increased as the reaction time or oxidant concentration increased. Images shown are at half-height of the hydrogel cylinder as found by *z*-sectioning. The dark ring found in 50 mM, 50 min and 100 mM, 25 min is most likely due to the hydrogel tearing during the deswelling process, causing two polymer domains to form.

**Chart 1. Chemical Structures of Hydrogel Components**[a]

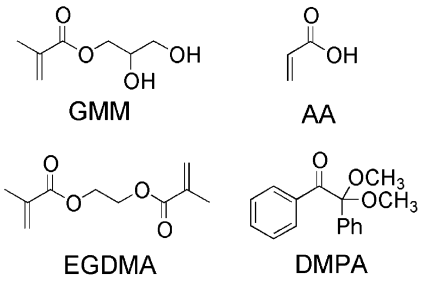


[a] Monomers: glycerol monomethacrylate (GMM) and acrylic acid (AA). Cross-linker: ethylene glycol dimethacrylate (EGDMA). Photoinitiator: 2,2-dimethoxy-2-phenyl-acetophenone (DMPA).

consistent solution for the electrical potential, $\psi$, and the concentrations of the ions, $c_k$. The concentration of the final oxidized product (i.e., aldehyde) is then computed from the chemical rate (eq 12) and the oxidation depth obtained from the concentration profile of the aldehyde.

## Results and Discussion

**Preparation of Hydrogels.** Hydrogels consisting of a 3:1 GMM[33]:acrylic acid (AA) monomer mixture containing 1 mol % ethylene glycol dimethacrylate (EGDMA) as an inert cross-linker and 2,2-dimethoxy-2-phenylacetophenone (DMPA) as a photoinitiator (Chart 1) were successfully prepared in microchannels by the methods we have previously reported for other hydrogels.[11] The prepolymer solution was injected into a prefabricated glass microchannel and allowed to reach a quiescent state. A photomask containing a 400 $\mu$m circle was then positioned on top of the glass microchannel and exposed to UV light from a standard fluorescent microscope for 50 s. Remaining monomer was then flushed away with successive washes of water and methanol. The hydrogels were left to bathe in water, where they reached an equilibrium diameter of approximately 700 $\mu$m (Figure 3a). The prepared hydrogels had good mechanical strength and did not deform when subjected to high volumetric flow rates through the channel (>6.5 mL $min^{-1}$). Because of the acrylic acid in the polymer backbone, the hydrogels were pH-responsive and expanded (~1000 $\mu$m) when exposed to a pH 7.6 phosphate buffer.

**Oxidation Depth of Hydrogels.** The in situ surface modification of GMM-*co*-AA hydrogels was carried out using aqueous solutions of $NaIO_4$ to achieve the conversion of the GMM's 1,2-diol into the corresponding aldehyde. The reaction between $NaIO_4$ and 1,2-diols has been documented as a fast reaction that is mild enough to be used on living cells.[34,35] Owing to the mild and aqueous reaction conditions, this modification scheme was thought to be beneficial to the chemical integrity of the polymer backbone (i.e., no oxidative cleavage) and to the adhesive materials used in fabricating the microchannel. The aqueous oxidation conditions were also advantageous as no significant polymer reorganization at the surface was expected, as would occur in changing from aqueous to organic solvents and vice versa.

Oxidation of the GMM-*co*-AA hydrogels was optimized to achieve a thin, near-surface modification by systematically varying conditions including $NaIO_4$ concentration, flow rates, reaction times, and temperature. After the desired oxidation time was completed, excess water was flushed through the channel to remove residual oxidant and to stop the modification process. Derivitization with lucifer yellow was then used to quantitatively measure the oxidation depth. Lucifer yellow is a water-soluble fluorescent dye containing a carbohydrazide functional group that conjugates selectively to aldehydes.[36] Combining the fluorescent dye with a 100-fold excess of a nonfluorescent molecule (semicarbazide hydrochloride) in a pH 7.6 phosphate buffer provided conditions for the expansion and fluorescent labeling of the hydrogel. At this pH, the hydrogel expanded, which allowed for the fast diffusion of the dye into the polymer network. Following fluorescent labeling, the hydrogel was collapsed to near its original diameter with an acidic buffer (pH 2.05). Although surface reorganization occurs during the swelling and shrinking process, we assume the large depth of oxidation (>10 $\mu$m) makes

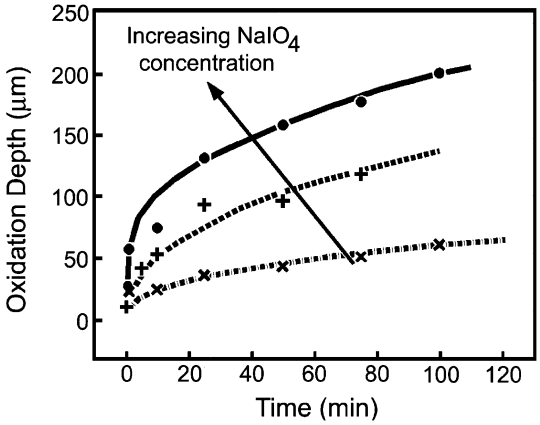


**Figure 5.** Experimental and simulated data for hydrogel oxidation as a function of reaction time. Experimental data points are for 10 (×), 50 (+), and 100 mM (●). Simulations are shown by solid (10 mM), dashed (50 mM), and dashed−dot (100 mM) lines.

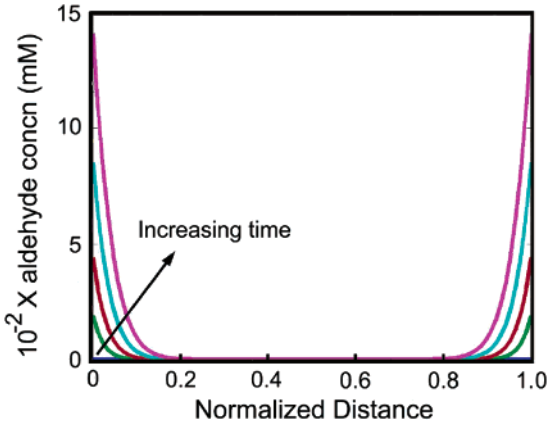


**Figure 6.** Simulation of a 50 mM $NaIO_4$ oxidation and the buildup of aldehyde concentration [D] as a function of position along the hydrogel diameter as the reaction time is increased. Time points (in min): 0 (blue), 16 (dark green), 36 (orange), 64 (light green), 100 (red).

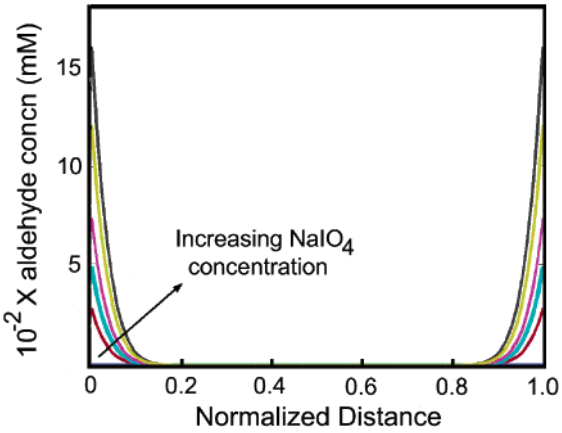


**Figure 7.** Simulation of a hydrogel oxidized for 10 min with increasing concentrations of $NaIO_4$ as a function of position along the hydrogel diameter. $NaIO_4$ concentrations (in mM): 0 (blue), 20 (orange), 40 (green), 80 (red), 120 (yellow), 180 (black).

this effect insignificant. Confocal microscopy was then employed to visualize the fluorescent probes located throughout the structure (Figure 3b). The middle height of the hydrogel cylinder was used for oxidation depth measurements, as the top and bottom are in contact with the glass cartridge. This contact caused the middle of the hydrogel to have a slightly increased diameter (~20 $\mu$m) compared to the top and bottom which is most likely caused by the physical contact between the hydrogel and the glass surface. The middle of the hydrogel cylinder, which was the widest cross section with the most fluorescence intensity, was found by scanning the *z*-axis. As a control, a nonoxidized hydrogel was subjected to the fluorescent labeling solution but showed no visible fluorescence, indicating that all nonconjugated lucifer yellow was washed from the hydrogel.

Because of the porosity of the hydrogel, the depth of oxidation is expected to be controlled by both the diffusion of $NaIO_4$ into the polymer network as well as the oxidation rate. The effect of concentration and time on the hydrogel oxidation was investigated by subjecting a series of hydrogels to systematic changes in reaction conditions. Three concentrations of $NaIO_4$ were chosen so that the oxidation depth could be monitored over a reasonable amount of time (1−100 min) without fully oxidizing the sample. The oxidation depth was defined as the average distance into the hydrogel (two sides) that contained visible fluorescence. As shown in Figure 4, increasing the concentration of $NaIO_4$ or increasing the reaction time led to significant changes in the oxidation depth. The oxidation depth could be controlled between 30 and 200 $\mu$m (Figure 5) by simply changing the $NaIO_4$ concentration or subjecting the hydrogel to longer oxidation times. As the $NaIO_4$ diffuses through the hydrogel, it is consumed and further reactions are negated; however, an increase in the concentration or exposure time allowed for a larger flux of $NaIO_4$ to enter the gel, allowing for more oxidation to occur. The increase in oxidation depth was also consistent with the chemical reaction's dependence on both the diol and $NaIO_4$ concentrations.[37]

As shown by the concentration and time dependent oxidation of the hydrogels, the diffusion of $NaIO_4$ into the polymer matrix is competitive with the rate of the reaction. Because the hydrogel is located within a microchannel and the oxidizing solution is being flown around it, a second diffusion term (convection) was evaluated. Convection is the transport of molecules arising from the motion of a streaming fluid,[38] which can replenish reactants that are consumed or diffuse away. Both diffusion and convection are additive and combine to affect the $NaIO_4$ concentration profile. To find the significance of convection, flow rates were varied over an order of magnitude (0.32−5.0 mL $min^{-1}$); however, hydrogels subjected to increased flow rates showed no sign of larger oxidation depths (see Supporting Information). Given the absence of an apparent convection process, this term was omitted from the modeling portion.

Simulations of the oxidation process were accomplished by combining the Nernst−Planck, Poisson, Arrhenius, and oxidation rate equations. These simulations compared well with experimental data (Figure 5) and could be used to predict the concentration of aldehyde functionality in the hydrogel at various locations. Using the initial concentration of 1,2-diol in the hydrogel (1.75 M) and a calibration curve of fluorescence intensity vs concentration of lucifer yellow (see Supporting Information), the aldehyde concentration profile could be obtained.[30] The simulated oxidation of a GMM-*co*-AA hydrogel with a 50 mM $NaIO_4$ solution and increasing reaction time (1−100 min) is shown in Figure

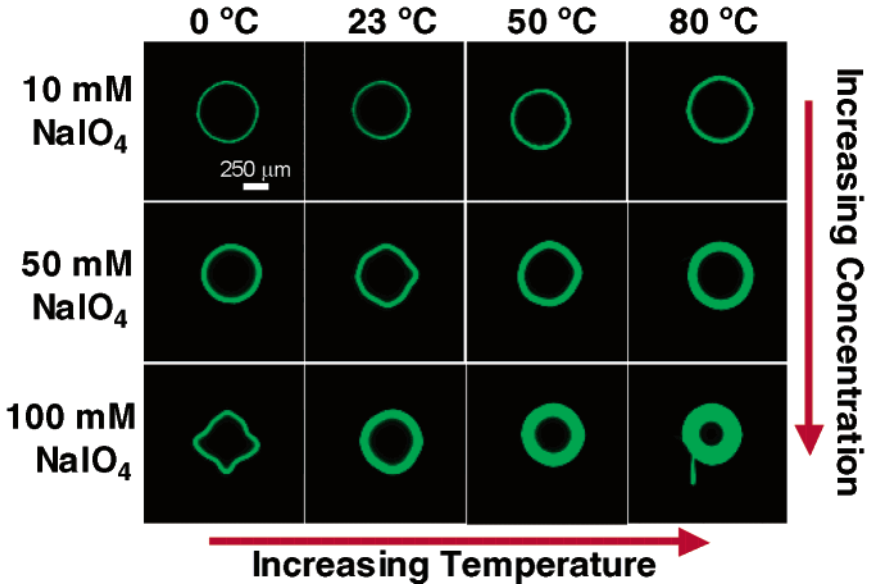


**Figure 8.** Confocal images of 12 lucifer yellow-labeled hydrogels oxidized with different $NaIO_4$ concentrations and various temperatures. Images shown are at half-height of the hydrogel as found by *z*-sectioning. Irregular shaped hydrogels were a consequence of the deswelling process. The effect may be due to increased interactions between the glass and the modified hydrogels.

6. The concentration of aldehyde is plotted against the normalized distance, which is relative to the diameter of the hydrogel. As expected, the concentration of aldehyde is maximized near the hydrogel−solution interface and decreases toward the center of the hydrogel. The modeling indicates that about 87% of the diol at the hydrogel−solution interface is oxidized when a 50 mM $NaIO_4$ solution is flowed through the channel for 100 min. Similarly, a simulated 10 min oxidation of a GMM-*co*-AA hydrogel with increasing concentrations of $NaIO_4$ is shown in Figure 7. As expected, the increase in ion flux due to increased concentrations of $NaIO_4$ resulted in increased oxidation over the reaction time. The simulation indicates that a 180 mM $NaIO_4$ solution and a 10 min oxidation time will oxidize about 92% of diol to aldehyde at the hydrogel−solution interface. These simulations show that although we can achieve high oxidation concentrations at the hydrogel−solution boundary, diffusion of the oxidant into the hydrogel diminishes the oxidation gradient at extended oxidation times.

The effect of temperature on the hydrogel oxidation was also explored. Heating or cooling of the hydrogel was accomplished by submersing the microchannel in a water bath at the desired temperature. Four reaction temperatures (0, 23, 50, and 80 °C) and three $NaIO_4$ concentrations (10, 50, and 100 mM) were utilized for the hydrogel oxidations over a 10 min period (Figure 8). As expected, the oxidation depth of the hydrogel increased when higher temperatures were used (Figure 9). These data was modeled by including the Arrhenius equation, and the results are consistent with the higher oxidation depth being primarily caused by an increased oxidation rate.

**Immobilization of FITC-BSA to Hydrogel Surface.** To demonstrate the utility and versatility of this hydrogel system for biomolecule immobilization, we have employed reductive amination to conjugate proteins displaying lysine residues to aldehydes localized on the perimeter of a patterned hydrogel (Figure 10a).[15] Fluorescein-labeled bovine serum albumin (FITC-BSA) protein was conjugated to 3:1 GMM-*co*-AA hydrogels that were oxidized with $NaIO_4$ for 10 min. A pH 7.4

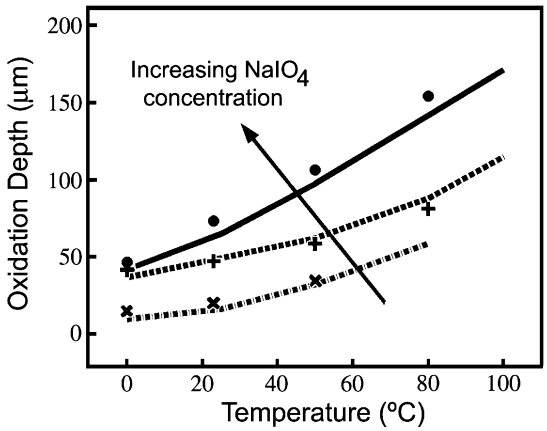


**Figure 9.** Experimental and simulated data for hydrogel oxidation as a function of temperature. Oxidations were carried out for 10 min. $NaIO_4$ concentrations: 10 (×), 50 (+), and 100 mM (●). Simulations are shown by solid (10 mM), dashed (50 mM), and dashed−dot (100 mM) lines.

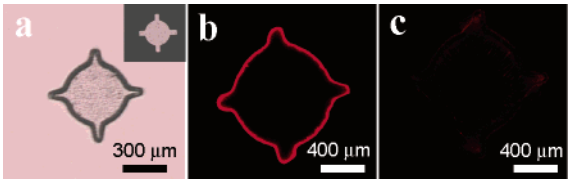


**Figure 10.** Optical micrograph of a GMM-*co*-AA hydrogel with a spike-circle design (a). Reductive amination of FITC-BSA to a $NaIO_4$ oxidized hydrogel (b) and a nonoxidized hydrogel (c) was attempted using $NaCNBH_3$. Only the oxidized hydrogel retained the fluorescent protein after washing.

phosphate buffer containing 1.5 mg $mL^{-1}$ FITC-BSA and 10 mg $mL^{-1}$ $NaCNBH_3$ was introduced into the microchannel. These conjugation conditions were beneficial in speeding the diffusion of the protein into the polymer network, owing to the swelling of the hydrogel. After washing with phosphate buffer to remove nonconjugated FITC-BSA, confocal microscopy was used to evaluate the location of the protein. The oxidized hydrogels conjugated with FITC-BSA showed fluorescence (Figure 10b) near the surface similar to hydrogels labeled with lucifer yellow. Control hydrogels, GMM-

*co*-AA hydrogels not oxidized with $NaIO_4$ but subjected to the reductive amination with FITC-BSA, showed little fluorescence under the same visualization conditions (Figure 10c). These results suggest that the aldehyde containing hydrogels are applicable to many of the current techniques employing gluteraldehyde as a linker molecule. These applications include the immobilization of proteins for bioreactors or biosensors onto a unique, pH-responsive hydrogel scaffold.

## Conclusions

Through simple organic transformations, hydrogel surfaces were transformed into specialized materials capable of chemoselective ligation of fluorescent dyes and proteins. These surface-modified hydrogels offer the ability to create materials for biosensing, biocatalysis, or controlled drug delivery once modified with biologically relevant materials. Here we have demonstrated the preparation and characterization of pH-responsive hydrogels capable of chemoselective ligation at their surface in a fast and simple way. An in situ photopolymerization of GMM-*co*-AA monomers created pH-responsive hydrogel cylinders which could be oxidized with $NaIO_4$ under mild conditions. The oxidation depth was controlled between 30 and 200 $\mu$m by varying the concentration, reaction time, and temperature of the oxidation step. A mathematical model has been developed to capture the oxidation phenomena, and the simulations compare well with the experimental results. The depth of oxidation was observed to be controlled by both the diffusion of the periodate reagent into the hydrogel as well as the reaction of $NaIO_4$ with the diol inside the hydrogel matrix. The model shows that the oxidizing parameters can be adjusted to achieve the desired degrees of oxidation; however, the diffusion−reaction pathway creates a tradeoff between achieving a sharp oxidation profile or a high oxidation conversion. Fluorescently labeled BSA was successfully reacted with the oxidized hydrogel surface providing the initial platform for hydrogels capable of selective bioconjugations.

**Acknowledgment.** The authors thank Cynthia Smith for valuable discussions and support. This material is based upon work supported by the National Science Foundation under Grant 0106608 and by DARPA, AFRL, Air Force Command, and USAF under Agreement F 30602-00-1-0570.

**Supporting Information Available:** Experimental section, calibration curve for lucifer yellow concentration, effect of convection on oxidation depth, and a table containing the parameters used in the modeling portion. This material is available free of charge via the Internet at http://pubs.acs.org.

## References and Notes

(1) Chan, C.-M. *Polymer Surface Modification and Characterization*; Hanser: New York, 1994.
(2) Lee, K.-W.; McCarthy, T. J. *Macromolecules* **1988**, *21*, 2318−2330.
(3) Costello, C. A.; McCarthy, T. J. *Macromolecules* **1987**, *20*, 2819−2828.
(4) Franchina, N. L.; McCarthy, T. J. *Macromolecules* **1991**, *24*, 3045−3049.
(5) Sevcik, S.; Vacik, J.; Chmelikova, D.; Smetana, K., Jr. *J. Mater. Sci.: Mater. Med.* **1995**, *6*, 505−509.
(6) Kiser, P. F.; WIlson, G.; Needham, D. *Nature (London)* **1998**, *394*, 459−461.
(7) Sackmann, E. *Science* **1996**, *271*, 43−48.
(8) Jin, T.; Pennefather, P.; Lee, P. I. *FEBS Lett.* **1996**, *397*, 70−74.
(9) Kiser, P. F.; Wilson, G.; Needham, D. *J. Controlled Release* **2000**, *68*, 9−22.
(10) Kraft, M. L.; Moore, J. S. *J. Am. Chem. Soc.* **2001**, *123*, 12921−12922.
(11) Beebe, D. J.; Moore, J. S.; Yu, Q.; Liu, R. H.; Kraft, M. L.; Jo, B. H.; Devadoss, C. *Proc. Natl. Acad. Sci. U.S.A.* **2000**, *97*, 13488−13493.
(12) Lemieux, G. A.; Bertozzi, C. R. *Trends Biotechnol.* **1998**, *16*, 506−513.
(13) Hild, G. *Makromol. Chem.* **1976**, *177*, 1947−1972.
(14) Tam, J. P.; Yu, Q.; Miao, Z. *Biopolymers* **1999**, *51*, 311−332.
(15) Hermanson, G. T. *Bioconjugate Techniques*; Academic Press: San Diego, 1996.
(16) Buist, C. J.; Bunton, C. A. *J. Chem. Soc.* **1954**, 1406−1413.
(17) Taylor, J. E.; Masui, H. *J. Phys. Chem. A* **2001**, *105*, 3532−3535.
(18) Malmivuo, J.; Plonsey, R. *Bioelectromagnetism: Principles and Applications of Bioelectric and Biomagnetic Fields*; Oxford University Press: New York, 1995.
(19) Tien, H. T.; Leitmannova, A. O. *Membrane Biophysics as Viewed from Experimental Bilayer Lipid Membranes*; Elsevier: New York, 2000.
(20) Jeans, J. H. *The Mathematical Theory of Electricity and Magnetism*; Cambridge University Press: London, 1911.
(21) Berry, R. S.; Rice, S. A.; Ross, J. *Physical Chemistry*; John Wiley and Sons: New York, 2001.
(22) Taylor, J. E. *J. Am. Chem. Soc.* **1953**, *75*, 3912−3917.
(23) Taylor, J. E. *J. Phys. Chem. A* **1995**, *99*, 59−63.
(24) Bruce, P. G. *Solid State Electrochemistry*; Cambridge University Press: New York, 1995.
(25) Nussbaum, J. H. Electric Field Control of Mechanical and Electromechanical Properties of Polyelectrolyte Gel Membranes. Ph.D. Thesis, Massachusetts Institute of Technology, Cambridge, MA, 1996.
(26) Mackie, J. S.; Meares, P. *Proc. R. Soc. London, Ser. A* **1955**, *232*, 510−518.
(27) Ende, M. T.; Hariharan, D.; Peppas, N. A. *React. Polym.* **1995**, *25*, 127−137.
(28) Amsden, B. *Macromolecules* **1998**, *31*, 8382−8395.
(29) De, S. K.; Aluru, N. R.; Johnson, B.; Crone, W. C.; Moore, J. S. *J. Microelectromech. Syst.* **2002**, *11*, 544−555.
(30) The effective molarity of the diol was calculated using the known densities of the monomers and the known volume change after the hydrogel swelled in water.
(31) Jin, X.; Li, G.; Aluru, N. R. *CMES* **2001**, *2*, 447−462.
(32) Aluru, N. R.; Li, G. *Int. J. Num. Methods Eng.* **2001**, *50*, 2372−2410.
(33) Deschenaux, R.; Stille, J. K. *J. Org. Chem.* **1985**, *50*, 2299−2302.
(34) Tolvanen, M.; Gahmberg, C. G. *J. Biol. Chem.* **1986**, *20*, 9546−9551.
(35) Norgard, K. E.; Han, H.; Leland, P.; Kriegler, M.; Varki, A.; Varki, N. M. *Proc. Natl. Acad. Sci. U.S.A.* **1993**, *90*, 1068−1072.
(36) Stewart, W. W. *Nature (London)* **1981**, *292*, 17−21.
(37) Buist, G. J.; Bunton, C. A. *J. Chem. Soc. B* **1971**, 2117−2128.
(38) Atkins, P. W. *Physical Chemistry*; W.H. Freeman and Co: New York, 1994.

MA035166+